*Ninth International Conference on CFD in the Minerals and Process Industries*
*CSIRO, Melbourne, Australia*
*10-12 December 2012*

# GAS-POWDER FLOW SIMULATION IN AN ELECTROSTATIC PRECIPITATOR WITHOUT ELECTRIC FIELD

**Baoyu GUO[1]*, Aibing YU[1], Lifeng LI[2], Xinglian YE[2]**

[1]Lab for Simulation and Modelling of Particulate Systems, School of Materials Science and Engineering, University of New South Wales, Sydney, NSW 2052, AUSTRALIA

[2]Experimental and Research Central, Fujian Longking Co., Ltd. Longyan, 364000, CHINA

*Corresponding author, E-mail address: baoyu@unsw.edu.au

## ABSTRACT

Emission of submicron particulate matters to the environment is of major health concern. Understanding of flow phenomena and their interaction with electric fields, together with complicated geometric structures in the Electrostatic Precipitators (ESP) is essential to the effective removal of such fine particles by this device. While previous works in this area are largely confined to the local region of the electrode and based on simple geometric/ boundary conditions (e.g., 2-D, uniform inlet velocity), attempts to predict the overall collection performance of practical ESP device with typical internal components are few, which is particularly useful to process design and optimization. In the current paper, the turbulent gas-powder (with particle size 0.1-75 microns) flow in an ESP is studied numerically using the Eulerian-Lagrangian method without considering an electric field. The ESP considered comprises typical internal components, such as a large angle diffuser, two perforated plates with directing vanes, two separate collection chambers, partition baffles in the hoppers. The simulated results are compared with experimental measurements in terms of gas flow velocity, particle concentration and gravitational precipitation rate.

## NOMENCLATURE

$C_C$ Cunningham slip correction factor
$C_D$ drag coefficient
d diameter
f porosity of perforated plate
$\mathbf{f}_{dis}$ particle dispersion force
**g** gravity
m mass
*P*,*p* pressure
Re Reynolds number
$U_0$ inlet gas velocity to the diffuser
u,**u** velocity
v normal velocity to perforated plate

$\rho$ density
$\mu$ dynamic viscosity
$\lambda$ mean free path

subscript
*g* *gas*
*p* *particle*

## INTRODUCTION

Fine and ultrafine particles are suspected to have a considerably stronger impact on human health than coarse particles. In spite of theoretical, experimental and numerical studies over the years, the fundamental problems still remain, i.e., how to enhance fine particle collection efficiency and to optimise the design of the specific particle removal device at the emitting sites. Mathematical modelling provides a cost-effective tool to understand the particle flow and to thus improve the particle collection efficiency in ESP, a widely-used particulate removal device. Among different numerical approaches, the Eulerian-Lagrangian method has been widely accepted for simulation of micro-size suspended particles flow with low solid loading in ESP applications (Nikas et al., 2005; Soldati et al., 1993; Zhang et al., 2005) as well as in other applications such as cyclone (Wang et al., 2006) and blast furnace (Guo et al., 2005). Considering the localized nature of turbulence, Soldati et al. (1993) attempted direct numerical simulation to study the particle dispersion in duct flow at a Reynolds number of 6,000. Choi and Fletcher (1998) considered distributed particle sizes without turbulent dispersion.

The studies outlined above are largely limited to the local region of the electrode and are based on simple geometric/ boundary conditions (e.g., 2-D, uniform inlet velocity). In fact, the gas-particle flow behaviour in every part of the whole system will affect the collection efficiency. Galliberti (1998) presented a method, where the precipitator modelling and the assessment of the cleaning efficiency are based on physical principles only. A full-scale simulation of an ESP chamber with hoppers and a plate distributor (Varonos et al, 2002) allows the investigation of the gas flow profile at the collection section inlet. In these large-scale ESP modelling, no information has been given on the collection mechanism based on the physics of particle-wall interactions.

A pilot scale ESP unit test rig is available in Longking Co Ltd. Based on this rig, the current aim is to develop a CFD model for macroscopic study, particularly for gas-suspended particle flow without an electric field. This is an essential step towards developing a full ESP process model, because (a) the gas-particle flow modelling approach should be checked first; (b) the boundary flow conditions of the electric regions are required when the transport phenomena within the electric field are to be solved. The current case considers most internal

mechanical structures in a typical ESP, thus giving realistic bulk flow distribution and boundary flow conditions for electric field zones. The simulation results are compared with the measured data.

## MODEL DESCRIPTION

The gas-particle flows are simulated using mixed Eulerian-Lagrangian method. This means that the gas flow is solved using a continuum (Navier-Stokes equation) method based on the Eulerian grid, whereas the particle flow uses a statistical approach to track a large number of samples of discrete particles. In a steady state simulation, the particle trajectories are integrated in sequence, without any interaction between them, therefore the Lagrangian method is more accurate for a low solid particle loading system as is the case for the flue gas from coal-fired power plant from pulverised coal injection. The equation of particle motion is written as:

$$m_{\mathrm{p}} \frac{d\mathbf{u}_{\mathrm{p}}}{dt} = C_D \pi d_p^2 \frac{\rho}{8} |\mathbf{u}_{\mathrm{g}} - \mathbf{u}_{\mathrm{p}}| (\mathbf{u}_{\mathrm{g}} - \mathbf{u}_{\mathrm{p}}) + \mathbf{f}_{\mathrm{dis}} + m_{\mathrm{p}} \mathbf{g} \quad (1)$$

The major forces on the particle include drag force, turbulence dispersion force and gravity. The drag coefficient is calculated as follows:

$$C_{\mathrm{D}} = \max(0.44, \frac{24}{C_{\mathrm{c}} Re_{\mathrm{p}}} (1 + 0.15 Re_{\mathrm{p}}^{0.687})) \quad (2)$$

$$C_C = 1 + 2.52\lambda / d_p \qquad \text{for } d_{\mathrm{p}} > 0.1\mu\mathrm{m} \quad (3)$$

$$C_C = 1 + (\lambda / d_p)[2.34 + 1.05\exp(-0.39 d_p / \lambda)] \qquad \text{for } d_{\mathrm{p}} < 0.1\mu\mathrm{m} \quad (4)$$

The standard k-ε turbulence model is used for gas phase. For the particle phase, the eddy interaction model (Gosman and Ioannides, 1983) is applied for particle dispersion.

Particles colliding with the hopper walls will be collected after a sufficiently long time (currently twice the mean gas residence time). Otherwise they rebound and will be further tracked. The properties of the particles collected, such as particle size, mass and number flow rate, are recorded in the user routines for post processing.

## EXPERIMENT

A 1:10 scaled test rig is chosen as a case for modelling and experiment work on the gas-powder flow (refer to Figure 2). The inlet pipe includes a transition section linking a circular bend pipe (280mm ID) to the square duct (400x400mm). In the diffuser, there are two 3mm-thick perforated plates with open porosity $f$ = 0.454 and 0.386 respectively. The orifice diameter on the perforated plate is 27mm. Several vertical guide vanes are attached perpendicularly to each perforated plate on the backside. A significant gap exists between the perforated plate and the diffuser wall at the bottom edge of the plates. A solid seating plate (100mm high) is used for hanging the perforated plate to the top wall. Between the two stage collection field, there is a lateral barrier (cylinder and baffle), above which the measurements are made. Two partition baffles are placed vertically in the first and last hoppers respectively. The particle size distribution (fly ash from power plant) is shown in Figure 1. The median diameter by volume is about 18 μm for this sample. Gas velocity is measured using a thermal anemometer (KANOMAX A531) at an array of points in the test section. Suspended particles passing these points are sampled and filtered using a collection tube at equal gas velocity and weighed over a certain time to calculate particle concentration. The overall particle weight accumulated in the hoppers is used to calculate the overall collection rate.

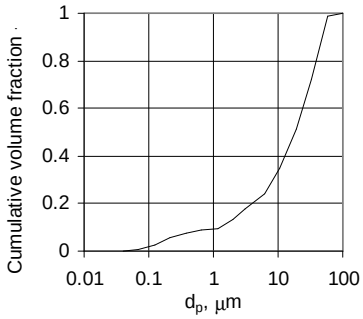


**Figure 1**: Particle size distribution provided

## MODEL CONDITIONS

Due to the geometric symmetry of the ESP body, only one half of the ESP is considered for the simulation domain as shown in Figure 2, where the test section and a mesh of measurement points are also indicated. The perforated plate is treated as a porous jump surface boundary, and the pressure drop is calculated by an empirical equation,

$$\Delta \mathrm{P} = C_1 \frac{f}{Re} + C_2 \frac{\rho}{2} u_n \max(u_n, 0.66u_n + 0.3u) \quad (5)$$

where $u$ is the total velocity value and $u_n$ is the normal velocity to the plate. The constants $C_1$=40 and $C_2$ is evaluated according to Idelchik (1996).

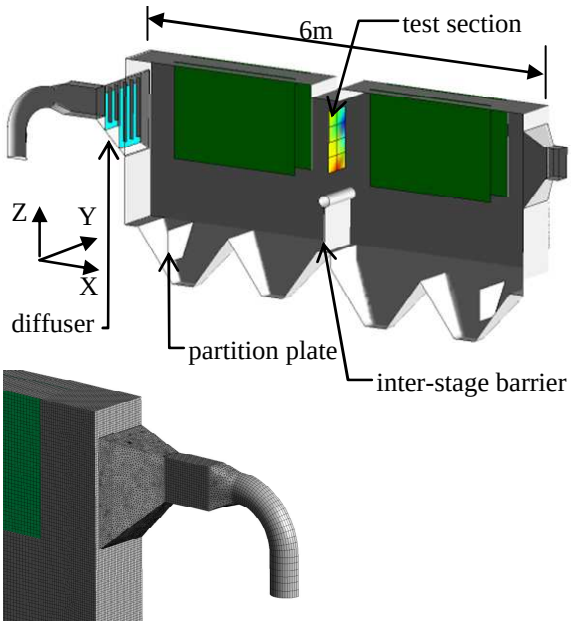


Figure 2: Model geometry and part of the mesh

The density for the powder particles is set as 2000 kg $m^{-3}$. The particles are injected randomly over the inlet, with the same velocity as gas flow.

## RESULTS

### Typical Gas flow

In the base case, the entry gas velocity to the diffuser is about 10 m/s, corresponding to an average velocity of 1m/s in the test section. The gas flow is found to be complicated due to the geometric complexity. In the inlet duct, a biased recirculation zone appears in the lower part of the square duct section due to the upstream bend and the expansion. There is a jet flow through the gap between the perforated plates and the lower inclined wall. The streamlines in the whole domain shows numerous eddies (Figure 3), even at the position of the first collecting plate, which deviates from the assumed plug flow. A reverse flow may even occur across the second perforated plate at the upper part.

An iso-surface in Figure 4 shows that a jet flow from the inlet, after the flow distributor (e.g., perforated plates), is directed downward rather than going straight forward. This jet flow not only provides a momentum to the above recirculation, but also has an implication to the particle flow, as it carries the particles towards the first hopper (facilitating deposition), and may also entrain some deposited fines into the flow (adverse effect).

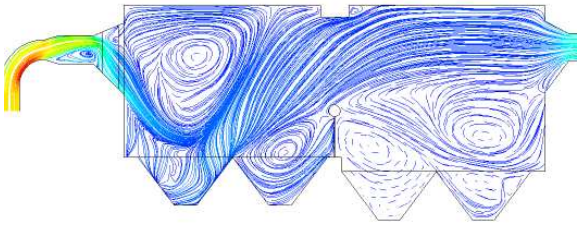

**Figure 3**: Mean gas flow streamlines on the symmetry plane (with color scaled to the velocity value).

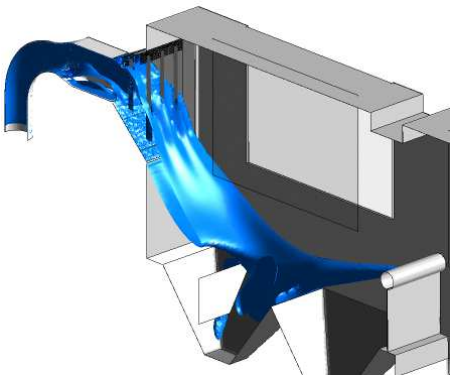

**Figure 4**: An isosurface of velocity (3m/s) showing a high velocity jet region.

Detailed comparison between the model prediction and our own measurement (unpublished data) is made in terms of the vertical line profiles (Figure 5), where Line-1 is close to the side wall and Line-3 is close to the symmetry plane. The match in the trend looks to be satisfactory. Good agreement is achieved near the wall (Line-1), while the velocity near the symmetry plane (Line-3) is over-predicted by about 30% compared with the measured one.

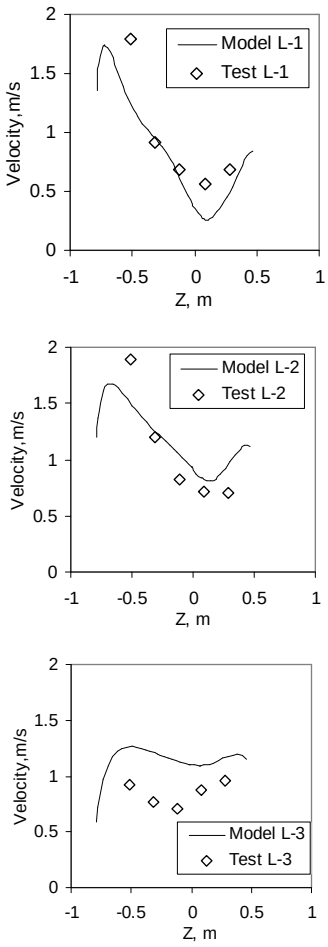


**Figure 5**: Comparison of gas velocity profiles.

### Particle Flow

Figure 6 shows the trajectories of particles respectively for the cases with and without considering the particle dispersion force. It can be seen that the inclusion of particle dispersion makes the particle trajectories more chaotic and spreads more widely. While some particles quickly exit the system through the outlet, the rest may be entrained in the eddies for long time. Those over-stayed particles are collected once they collide with the hopper walls. Other particles that neither escape nor collide with hopper walls have to be removed after a preset time limit /distance limit in the simulation, which introduces uncertainty when calculating the total collection rate (this will be discussed in the next section).

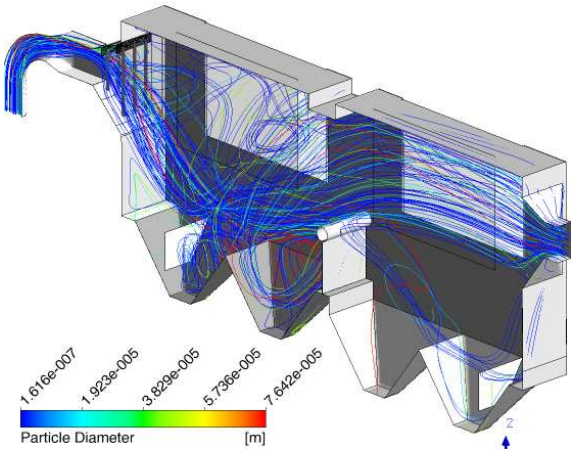


(a) Without particle dispersion

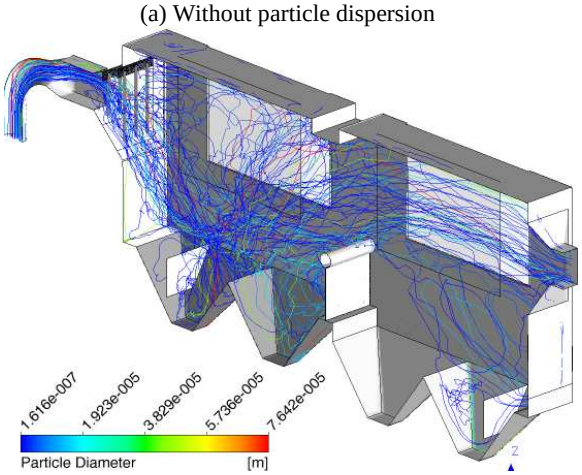


(b) With particle dispersion

**Figure 6**: Particle trajectories with colour scaled to the particle size.

Figure 7 shows the simulated distribution of particle phase volume fraction in the test section. High particle concentrations are found near the sidewall and at the bottom. Unlike the velocity profiles, the distribution of particle phase is usually not smooth, depending on the mesh resolution and the number of sample particles tracked. Increased number of particles and decreased mesh resolution make the distribution smoother. Typically 140000 particles are tracked and further increase has little effect on the result. The line profiles of the particle concentration are shown in Figure 8 (normalized by the initial value). No measurement could be made near the wall boundaries. It can be seen that the model and measurements are fairly close in value at most of measurement points. The line profiles for Line-1 and Line-3 are closer than for Line-2. However, the overall performance of the model is regarded as satisfactory in view of the complex nature of the present flow condition.

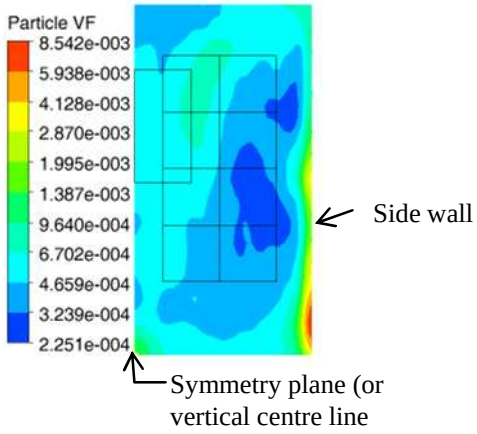


**Figure 7**: Mean particle volume fraction in the test section.

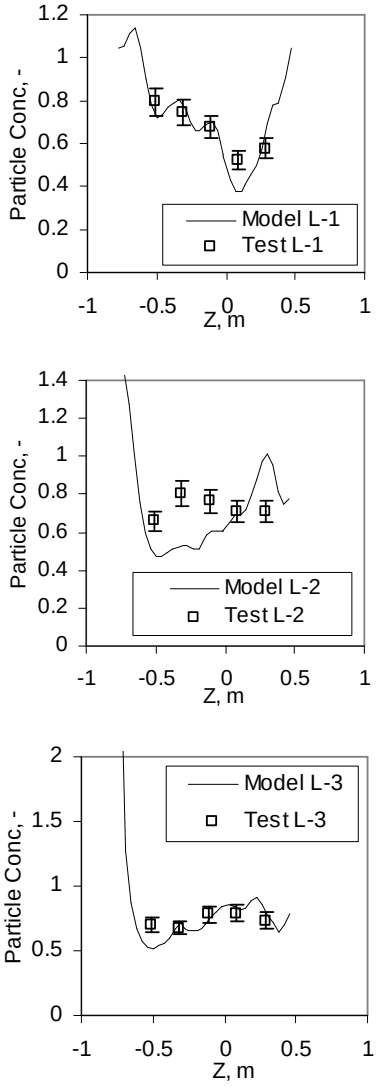


**Figure 8**: Profiles for particle mass concentration in the measurement plane.

### Effect of Inlet Velocity

Three different gas velocity conditions are considered in the range $U_0$=6-15 m/s, corresponding to the volume flow rates of 3778, 5597 and 8330 $m^3$/hr respectively. The gas velocity distributions, if normalized by their mean values, are similar for the three cases. For particle flow, the overall mass fraction collected from the hoppers (or the rate of settlement by gravity) is chosen as a quantity for model validation. As shown in Figure 9, the total collection fraction decreases as the gas flow rate increases, with a trend that is consistent with the measurement. Note, the error bars in the experiment data indicate the maximum and minimum values. However in the simulation result, the error bars indicate the maximum possible range of collection fraction determined by the exited fraction. This error is caused by the uncertain fates of the particles trapped in recirculation eddies. It can be seen that the lower limit of collection rate matches the measurement value very well. The mean particle size collected in the hoppers (30-40μm) is larger than the initial mean particle size (18μm), and also decreases slightly as the gas velocity increases (Figure 10).

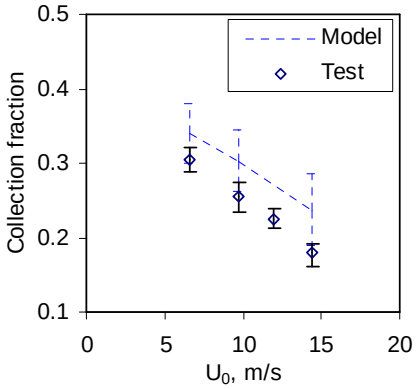


**Figure 9**: Collection rate for different inlet velocity.

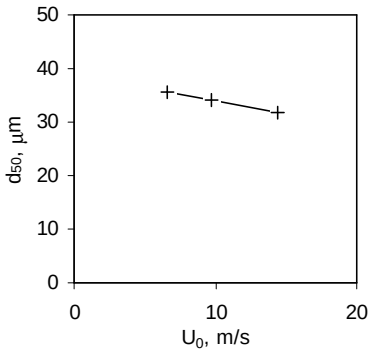


**Figure 10**: Predicted mean particle size collected for different inlet velocity.

### Effect of particle size

The collection rate differs for different particle size. As shown in Figure 11, it is nearly constant for particles below 10μm, increases as particle size increases above 10μm, until 100% collected above 100μm. The effect of particle dispersion is also obvious for different particle size, in that the curve for the case with turbulent dispersion is much smoother. Without the turbulent particle dispersion, the collection rate for small particles below 10μm tends to be under-predicted, while it may be over-predicted for intermediate size particles from 10 to 100μm. For large particles above 100μm, such effects will be negligible.

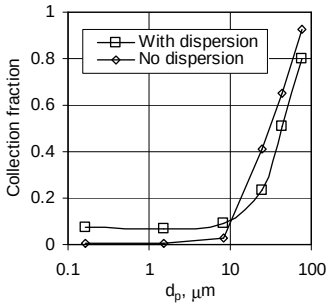


**Figure 11**: Collection fraction for different particle sizes.

## CONCLUSION

A CFD model of two-phase flow is developed based on the pilot scale ESP test rig. The gas-particle flow is simulated using Eulerian-Lagrangian method without considering an electric field. Simulation results show a very complex gas flow pattern with a large number of eddies and subsequently the complex particle flow. A large recirculation may exist even in the region of the first electric field.

Several parameters are considered, including gas flowrate, and particle size distribution. The simulated results are validated against experimental measurements in terms of gas flow velocity and particle concentration profiles, and particle collection rate in the hoppers.

A significant number of particles may be caught in the eddies and recirculate for a long time. Turbulent particle dispersion should be considered for better model prediction accuracy of particle flow. The total collection rate due to gravity has been accurately predicted. Therefore, the overall model performance is satisfactory and lays a solid foundation for further model development to include the electric field.

### Acknowledgement

Supports from Australian Research Council and Fujian Longking Co Ltd are gratefully acknowledged.

## REFERENCES

CHOI, B.S. and FLETCHER. C.A.J., (1998), “Turbulent particle dispersion in an electrostatic precipitator”, *Applied Math. Modelling* **22**: 1009-1021.

GALLIBERTI, I., (1998), “Recent advancements in the physical modelling of electrostatic precipitators”, *J.Electrostat*., **43**: 219–247.

GOSMAN, A.D. and IOANNIDES, E., (1983), “Aspects of computer simulation of liquid-fuelled combustors”, *J. Energy*, **7**: 482-490.

GUO, B.Y., ZULLI, P. ROGERS, H., MATHIESON, J.G. and YU, A.B., (2005), “Three-dimensional simulation of flow and combustion for pulverised coal injection”, *ISIJ Int*., **45**: 1272-1281.

IDELCHIK, I.E., (1996), Handbook of Hydraulic Resistance (3rd Ed.), Begell House, Inc.

NIKAS, K.S.P. VARONOS, A.A. and BERGELES, G.C., (2005), “Numerical simulation of the flow and the collection mechanisms inside a laboratory scale electrostatic precipitator”, *J. Electrostatics*, **63**: 423-443.

SOLDATI, A., ANDREUSSI, P. and BANERJEE, S., (1993), “Direct simulation of turbulent particle transport in electrostatic precipitators”, *AIChE J*., **39**: 1910-1919.

VARONOS, A.A., ANAGNOSTOPOULOS, J.S., BERGELES, G.C., (2002), “Prediction of the cleaning efficiency of an electrostatic precipitator”, *J. Electrostatics*, **55**: 111-133.

WANG, B., XU, D.L., CHU, K.W. and YU, A.B., (2006), “Numerical study of gas–solid flow in a cyclone separator”, *Applied Math. Modelling*, **30**: 1326-1342.

ZHANG, X., WANG, L. and ZHU, K., (2005), “Particle tracking and particle-wall collision in a wire-plate electrostatic precipitator”, *J. Electrostatics* **63**: 1057–1071.

 